Li et al. *Zool. Res.* 2024, 45(2): 233−241
https://doi.org/10.24272/j.issn.2095-8137.2023.190

ZR | Zoological Research

Article Open Access

Loss of SHROOM3 affects neuroepithelial cell shape through regulating cytoskeleton proteins in cynomolgus monkey organoids

Peng Li[1,2,#], Ting Zhang[1,2,#], Ruo Wu[1,2,#], Jun-Yu Zhang[1,2,#], Yan Zhuo[1,2], Shan-Gang Li[1,2], Jiao-Jian Wang[1,2], Wen-Ting Guo[1,2,*], Zheng-Bo Wang[1,2,*], Yong-Chang Chen[1,2,*]

[1] *State Key Laboratory of Primate Biomedical Research*, *Institute of Primate Translational Medicine*, *Kunming University of Science and Technology*, *Kunming*, *Yunnan* 650500, *China*

[2] *Yunnan Key Laboratory of Primate Biomedical Research*, *Kunming*, *Yunnan* 650500, *China*

ABSTRACT

Neural tube defects (NTDs) are severe congenital neurodevelopmental disorders arising from incomplete neural tube closure. Although folate supplementation has been shown to mitigate the incidence of NTDs, some cases, often attributable to genetic factors, remain unpreventable. The *SHROOM3* gene has been implicated in NTD cases that are unresponsive to folate supplementation; at present, however, the underlying mechanism remains unclear. Neural tube morphogenesis is a complex process involving the folding of the planar epithelium of the neural plate. To determine the role of SHROOM3 in early developmental morphogenesis, we established a neuroepithelial organoid culture system derived from cynomolgus monkeys to closely mimic the *in vivo* neural plate phase. Loss of SHROOM3 resulted in shorter neuroepithelial cells and smaller nuclei. These morphological changes were attributed to the insufficient recruitment of cytoskeletal proteins, namely fibrous actin (F-actin), myosin II, and phospho-myosin light chain (PMLC), to the apical side of the neuroepithelial cells. Notably, these defects were not rescued by folate supplementation. RNA sequencing revealed that differentially expressed genes were enriched in biological processes associated with cellular and organ morphogenesis. In summary, we established an authentic *in vitro* system to study NTDs and identified a novel mechanism for NTDs that are unresponsive to folate supplementation.

Keywords: Neural tube defects; SHROOM3; Neuroepithelial; Organoids; Cynomolgus monkey

INTRODUCTION

Neural tube defects (NTDs) are one of the most common birth defects, affecting approximately 1 in 1 000 newborns, with an even higher incidence in certain regions (Greene & Copp, 2014). These defects typically manifest as encephaloceles, anencephaly, or spina bifida at birth (Greene & Copp, 2014). Although periconceptional folate supplementation has been shown to significantly reduce the incidence of NTDs, between 30% and 50% of NTD cases remain unpreventable (Copp et al., 2013). Currently, there is no effective treatment for NTDs, imposing considerable financial and social burdens on families and healthcare systems.

Neurulation is a dynamic process regulated by a series of molecular and cellular events that culminate in the formation of a closed neural tube, which serves as the primordium of the entire central nervous system. Abnormalities in both genetic factors and nutrient metabolism are known contributors to NTDs (Copp et al., 2013). The *SHROOM3* gene has been identified as an essential component in neural tube closure. Loss-of-function mutations in this gene have been linked to folate-unresponsive NTDs in humans (Deshwar et al., 2020). Therefore, understanding why loss of SHROOM3 results in the occurrence of these defects is important for developing novel therapeutic strategies for untreatable NTDs.

Owing to ethical constraints, the utilization of human embryos in NTD research is limited, necessitating the employment of alternative animal models such as mice and *Xenopus* species. Despite the identification of more than 400 mouse genes as potential risk factors for NTDs, these animal models have not successfully elucidated the mechanisms

Received: 15 September 2023; Accepted: 21 November 2023; Online: 22 November 2023

Foundation items: This work was supported by the National Natural Science Foundation of China (81930121, 82125008 to Y.C.C.), National Key Research and Development Program of China (2018YFA0107902 to Y.C.C. and 2018YFA0801403 to Z.B.W.), Major Basic Research Project of Science and Technology of Yunnan (202001BC070001 to Y.C.C.), Natural Science Foundation of Yunnan Province (202102AA100053 to Y.C.C.)

[#]Authors contributed equally to this work

*Corresponding authors, E-mail: guowt@lpbr.cn; wangzb@lpbr.cn; chenyc@lpbr.cn

underlying human NTDs (Greene & Copp, 2014; Nikolopoulou et al., 2017), highlighting the need for more representative models. Non-human primates (NHPs) closely resemble humans in terms of physiology, nervous system architecture, and genetic background. In addition, *in vivo* and *in vitro* studies have demonstrated that the temporal patterns of early neurulation events, including neural tube closure, are notable analogous between monkeys and humans (Huang et al., 2021), thus establishing NHPs as ideal animal models for the study of NTDs.

In the present study, we explored the effects of SHROOM3 loss on the very early stages of embryonic development. Isolation of embryos at this developmental stage presents a significant challenge due to their very small size, requiring complete excision of the uterus. As an alternative approach, brain organoids offer a more accessible and ethical viable means to study early brain development. These organoids have been widely employed in research on various neurodevelopmental diseases, including Down syndrome, fragile X syndrome, Rett syndrome, Alzheimer's disease, and microcephaly (Chen et al., 2021; Gomes et al., 2020; Kang et al., 2021; Lancaster et al., 2013; Tang et al., 2021). Derived from pluripotent stem cells, brain organoids can mimic early brain development and reflect the proliferation, migration, and differentiation of neural progenitor cells. Thus, these organoids provide a robust, efficient, and reproducible platform for studying neurodevelopmental diseases and exploring the specific effects of different factors on neural tube development, while reducing animal use requirements and research material limitations.

In the present study, we established a neuroepithelial organoid culture system to explore the effects of SHROOM3 deficiency on neural tube development. Given that the efficiency of gene editing in embryonic stem cells (ESCs) is both low and labor-intensive, we generated *SHROOM3* knockout (KO) ESCs by editing monkey embryos rather than monkey ESCs or human ESCs/induced pluripotent stem cells (iPSCs). Our results demonstrated that SHROOM3 exerted significant impact on cell morphology by directly regulating the localization of fibrous actin (F-actin) and indirectly regulating the localization of myosin II and phospho-myosin light chain (PMLC) through Rho-associated coiled-coil kinase 1 (ROCK1). Inhibition of ROCK1 or F-actin replicated the *SHROOM3* KO phenotypes. RNA sequencing (RNA-seq) analysis revealed that differentially expressed genes (DEGs) were predominantly enriched in morphogenesis processes. Taken together, these findings indicate that *SHROOM3* plays a pivotal role in regulates cell shape at the very early stage of neural development, thereby expanding our understanding of the mechanisms underlying the development of NTDs.

MATERIALS AND METHODS

Ethics approval

This study strictly followed the Guidelines of the Experimental Animal Center of Kunming University of Science and Technology for the care and use of animals. All animal procedures were conducted in accordance with the ethical standards of the Experimental Animal Center of Kunming University of Science and Technology and were reviewed and approved by the Animal Ethics Committee (Approved No. KUST202301009).

Generation of *SHROOM3* KO ESC lines

Oocytes for generating both wild-type (WT) and *SHROOM3* KO embryos were obtained from the same cynomolgus monkey (*Macaca fascicularis*) via superovulation. Mature oocytes at the MII stage were transferred to 1 066 culture medium after intracytoplasmic sperm injection (ICSI) and cultured in 5% CO_2 at 37 °C. Approximately 2.5 h later, 100 ng/μL sgRNA (agacagtctatgacacccggagg) and 100 ng/μL Cas9 mRNA were injected into the cytoplasm of the fertilized oocytes Following injection, the oocytes were transferred to H9 culture medium and placed in an incubator for further culture. The culture medium was refreshed every other day. Upon reaching the blastocyte stage, the embryos were digested with protease for 30–40 s, then transferred to H9 culture medium and washed repeatedly until the zona pellucida was shed. Thereafter, the embryos were transferred to a dish containing feeder cells and cultured for an additional 4–5 days. On day 7, the inner cell mass was manually isolated using a needle and transferred to a dish with new feeder cells. The iPSC medium was replaced daily. Typically, the ESC clones became visible within 3 days. A small subset of these clones was selected for subsequent sequencing.

Stem cell culture and organoid differentiation

All ESC lines were fully characterized and cultured on irradiated mouse embryonic fibroblasts (MEFs) in a human iPSC medium consisting of Dulbecco's Modified Eagle Medium/Nutrient Mixture F-12 (DMEM/F12, Invitrogen, USA), 12% KnockOut Serum Replacement (KOSR, Invitrogen, USA), XF medium (Invitrogen, USA), 1×Glutamax (Invitrogen, USA), 1×MEM non-essential amino acids (NEAA) solution (Invitrogen, USA), 100 μmol/L βmercaptoethanol (Invitrogen, USA), and 10 ng/mL human basic fibroblast growth factor (FGF, PeproTech, USA), as described previously (Tan et al., 2021). Cynomolgus monkey-specific neuroepithelial organoids were generated based on previously described protocols (Zhu et al., 2016), with some modifications. Briefly, ESC colonies from cynomolgus monkeys were isolated from the feeder layer by the addition of 1 mg/mL collagenase. Subsequently, 20 000 cells were placed in 96-well U-shaped plates and cultured in iPSC medium supplemented with 10 μg/mL Y27632 (Selleck, USA) for 2 days to form embryoid bodies. On day 3, the organoids were embedded in Matrigel (Corning, USA) for 30 min in an incubator. Differentiation medium containing DMEM/F12, 1×N2 supplement, 1×B27 supplement (Invitrogen, USA), 100 μmol/mL β-mercaptoethanol (Invitrogen, USA), 1×MEM NEAA, 2.5 μg/mL insulin (Sigma, USA), 3 μmol/mL CHIR99021 (Selleck, USA), 5 μmol/mL SB431542 (Selleck, USA), vitamin C (Selleck, USA), and 10 ng/mL human basic FGF was added to the organoids. On day 12, the differentiated organoids were collected for analysis.

Immunocytochemistry

On day 12, the cynomolgus monkey-derived neuroepithelial organoids were fixed in 4% paraformaldehyde for 20 min, then washed three times with phosphate-buffered saline (PBS) at room temperature. The organoids were then embedded in optimal cutting temperature (OCT) compound and sectioned to a thickness of 10 μm (Leica, Germany). Sections were washed with PBS and permeabilized with 0.2% Triton-X for 1 h. Tissues were then blocked with a blocking solution consisting of 10% donkey serum in PBS containing 0.1% Tween-20 (PBST) for 30 min (Velasco et al., 2019). Primary antibodies (see Supplementary Table S1) were diluted with

the blocking solution and applied to the sections overnight at 4 °C. After washing with PBST three times, secondary antibodies diluted in the blocking solution were applied to the sections for 1 h at room temperature. Finally, the sections were counterstained with 4',6-diamidino-2-phenylindole (DAPI) and washed with PBST. Images were taken using a Leica TCS SP8 confocal microscope (Leica, Germany). Quantitative analyses were conducted on randomly selected rosette rings. Nucleus length and fluorescence intensity were measured using ImageJ software (NIH, USA) (Benito-Kwiecinski et al., 2021).

Western blotting and co-immunoprecipitation (Co-IP)

The cells were lysed with RIPA lysis buffer (Beyotime, China) supplemented with protein inhibitors (Trans company, China) and quantified using a BCA kit (Beyotime, China). The proteins were separated using sodium dodecyl sulfonate-polyacrylamide gel electrophoresis (SDS-PAGE) and transferred onto polyvinylidene difluoride (PVDF) membranes. The membranes were blocked with 5% nonfat milk at room temperature for 2 h, then incubated with primary antibodies at 4 °C overnight. After washing with PBST three times, the membranes were incubated with secondary antibodies at room temperature for 1 h. Immunoblot bands were detected using an enhanced chemiluminescence (ECL) detection system (Chemiscope 6200, China), quantified using ImageJ software, and normalized to vinculin. Co-IP was performed as described elsewhere (Burckhardt et al., 2021). Briefly, A/G magnetic beads (Beyotime, China), primary antibody, and protein lysates were gently rotated at 4 ℃ overnight. The immune complex was collected the next day for western blotting.

RNA isolation, reverse transcription-quantitative real-time polymerase chain reaction (RT-qPCR), and RNA-seq

RNA was reverse-transcribed using the SuperScript® III First-Strand Synthesis System (Invitrogen, USA). RT-qPCR was performed using the TaqMan™ assay (Invitrogen, USA). Each reaction was run in triplicate and analyzed following the Ct method, using glyceraldehyde-3-phosphate dehydrogenase (GAPDH) as the normalization control (Kang et al., 2021). For RNA-seq, total RNA was extracted using TRIzol reagent according to standard procedures. Samples were measured using a NanoPhotometer spectrophotometer and fragmented by the addition of fragmentation buffer. A six-base random primer was used to synthesize the first and second strands of cDNA. Qualified libraries were sequenced using the Illumina platform (PE150).

Statistical analysis

All data are shown as mean±standard deviation (*SD*). One-way analysis of variance (ANOVA) followed by Tukey's multiple comparison test or Student's *t*-test (two-tailed) was performed using GraphPad Prism (v9). Each experiment was performed with at least three independent biological replicates. Statistically significant results were determined at $P<0.05$. Quantitative analysis of cell area and nuclear length was performed using ImageJ software (Kang et al., 2021).

RESULTS

Loss of SHROOM3 led to morphological changes in neuroepithelial cells in cynomolgus monkey organoids

Oocytes for generating WT and *SHROOM3* KO embryos were obtained from the same cynomolgus monkey by superovulation. The *SHROOM3* KO embryos were generated by injecting mixtures of CRISPR/Cas9 system mRNA, coupled with specific sgRNA (Figure 1A) into embryos. Both WT and KO embryos were cultured to the blastocyte stage. Two WT and two *SHROOM3* KO ESC lines were then generated from the blastocytes. *SHROOM3* KO was confirmed by Sanger sequencing and western blotting (Figure 1B, C). The pluripotency of ESCs was confirmed by teratomas formation assay (Supplementary Figure S1A).

A 12-day organoid culture system was established to obtain neuroepithelial cells (Supplementary Figure S1B, C). Subsequent analyses showed that the RNA and protein levels of SHROOM3 decreased significantly with organoid development (Figure 1D–F). Notably, by day 35, RNA expression was reduced to half its level on day 12 (Figure 1D) and protein expression barely detectable, as confirmed by western blotting and immunofluorescent staining (Figure 1E, F). *In vivo*, SHROOM3 expression in the prefrontal cortex of seven-month-old cynomolgus monkeys was very low and difficult to detect (Figure 1G–I), suggesting a role for SHROOM3 during the early brain development. Consequently, we selected brain organoids from days 8 and 12, corresponding to the neuroepithelial stage, to further study the effects of SHROOM3. Results showed that loss of SHROOM3 affected both the shape and size of neuroepithelial cells. The WT neuroepithelial cells were larger and columnar in shape, whereas *SHROOM3* KO neuroepithelial cells were smaller and more oval-shaped (Figure 2A, B). Additional quantification revealed significant reductions in both nucleus length and cell area of *SHROOM3* KO neuroepithelial cells compared to WT cells (Figure 2C, D). The nucleus-to-cell area ratio showed no significant difference between the two groups (Figure 2E), suggesting synchronous changes in the nucleus and cell size. To assess the apical contractile capacity, the lumen area of the neuroepithelial cells was labeled with ZO-1. Results showed significant enlargement of the lumen in *SHROOM3* KO neuroepithelial cells compared to WT cells (Figure 2F, G), indicating that SHROOM3 deletion affects the apical contraction properties of neuroepithelial cells.

While folate supplementation cannot rescue phenotypes caused by loss of SHROOM3 in humans, it can affect the incidence of NTDs in *Shroom3* mutant mouse embryos (Marean et al., 2011). To investigate the potential of folate to ameliorate the phenotypic alterations induced by *SHROOM3* KO in early neuroepithelial development of cynomolgus monkeys, we administered 100 μmol/mL of folate to *SHROOM3* KO neuroepithelial cells (Chen et al., 2012). Based on wheat germ agglutinin (WGA) staining, folate supplementation did not improve cell shape and size (Supplementary Figure S2A–C) or the localization of cytoskeletal, polarity, and adhesion proteins (Supplementary Figure S2D–H), suggesting that folate administration cannot rescue the phenotypes induced by *SHROOM3* KO in cynomolgus monkeys.

Loss of SHROOM3 affected neuroepithelial cell shape by regulating myosin II, PMLC, and F-actin localization

As cytoskeletal proteins, such as F-actin, PMLC, and myosin II, play a crucial role in determining cell morphology (Zalewski et al., 2016), we next examined their expression and localization. In the WT group, the apical localization of F-actin, PMLC, and myosin II showed significant colocalization within

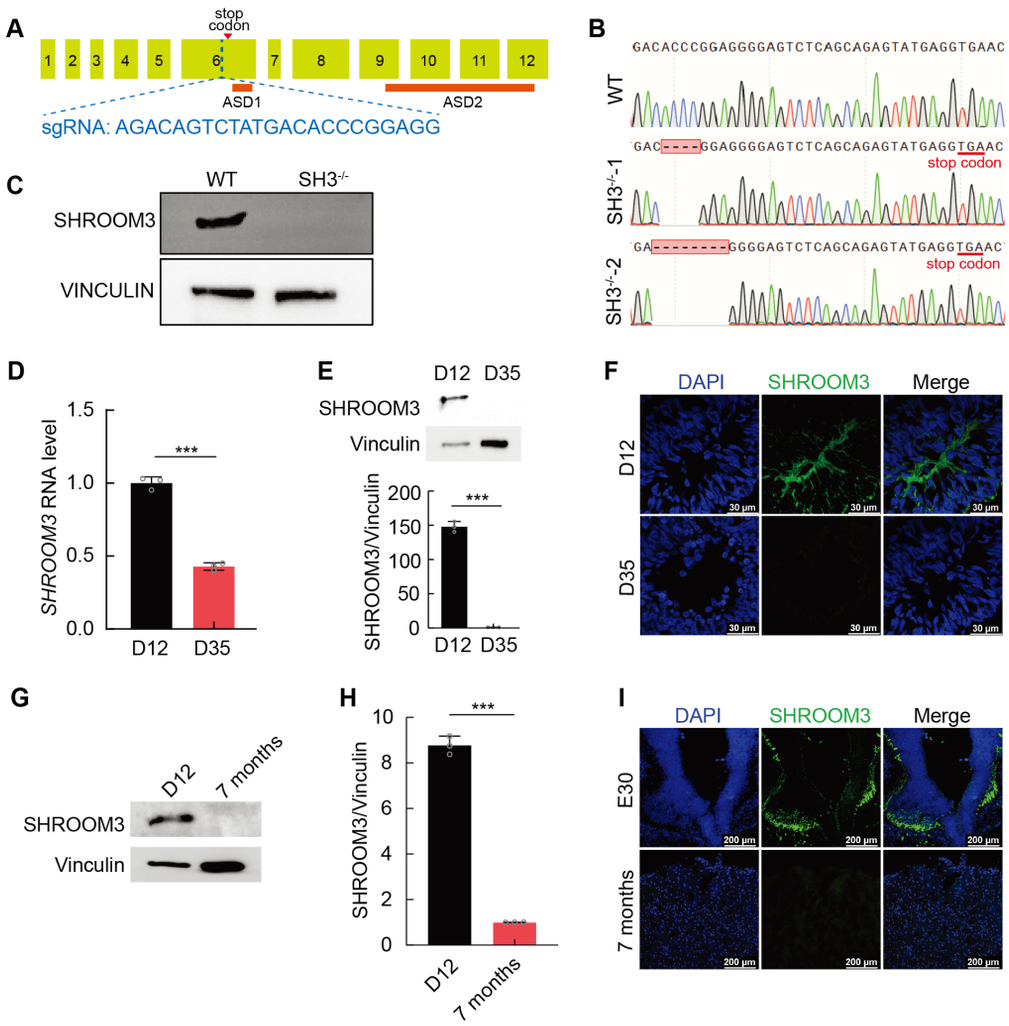

Figure 1 Expression of SHROOM3 at different times of brain development

A: Schematic depicting targeting strategy to generate *SHROOM3* KO embryos. B: Sanger sequencing of ESCs confirmed *SHROOM3* gene KO. C: Western blotting confirmed successful SHROOM3 KO. D: RT-qPCR of RNA level of *SHROOM3* in brain organoids on days 12 and 35, respectively. E: Western blotting of SHROOM3 in brain organoids on days 12 and 35, respectively. F: Representative immunofluorescence images of SHROOM3 in brain organoids on days 12 and 35, respectively. G, H: Western blotting of SHROOM3 in brain organoids on day 12 and prefrontal cortex of cynomolgus monkeys at seven months of age, respectively. I: Representative immunofluorescence images of SHROOM3 in neural tube of embryos at E30 and prefrontal cortex of cynomolgus monkeys at seven months of age, respectively. Data are mean±*SD*, ***: $P<0.001$.

neuroepithelial cells, a feature absents in the *SHROOM3* KO group (Figure 3A, B). Laminin was used as a marker for the basement membrane of neuroepithelial cells but showed no significant difference in localization (Figure 3C), suggesting that *SHROOM3* KO mainly affects the apical side of neuroepithelial cells. Co-IP assays, typically employed to identify protein-protein interactions, revealed that SHROOM3 directly interacted with F-actin (Figure 3D) but not with PMLC or myosin II (Figure 3E, G). SHROOM3 can interact with ROCK1 (Figure 3F) and indirectly regulate PMLC and myosin II through ROCK1.

Given the integral role of cell adhesion and polarity in normal neuroepithelial cell development (Smith et al., 2021), we investigated the potential effects of the *SHROOM3* gene on these cellular features by examining the expression and localization of N-cadherin, β-catenin, and ZO-1. No significant differences in the distribution of N-cadherin, β-catenin, and ZO-1 were observed between the WT and *SHROOM3* KO groups (Figure 4A–D). The Co-IP assay indicated that SHROOM3 directly recruited N-cadherin (Figure 4E) but not β-catenin (Figure 4F). Furthermore, no direct regulatory relationship was observed between SHROOM3 and ZO-1 (Figure 4G). Collectively, these findings suggest that loss of SHROOM3 affects neuroepithelial cell morphology by modulating the apical localization of myosin II, PMLC, and F-actinin but not N-cadherin, β-catenin, or ZO-1.

Inhibition of ROCK1 and F-actin affected neuroepithelial cell morphology

To determine whether SHROOM3 influences the morphology of neuroepithelial cells via ROCK1 and F-actin, we administered either 10 μL/mL of the ROCK1 inhibitor Y27632 or 2.5 μmol/mL of the F-actin inhibitor cytochalasin B (CB) at the beginning of neural differentiation. Inhibition of either ROCK1 or F-actin induced morphological changes similar to those in *SHROOM3* KO cells (Figure 5A–C). F-actin inhibition had a more pronounced impact and led to a reduced nucleus-to-cell area ratio (Figure 5A–D). Conversely, no significant difference in the nucleus-to-cell area ratio was found in the ROCK1 inhibition group (Figure 5D).

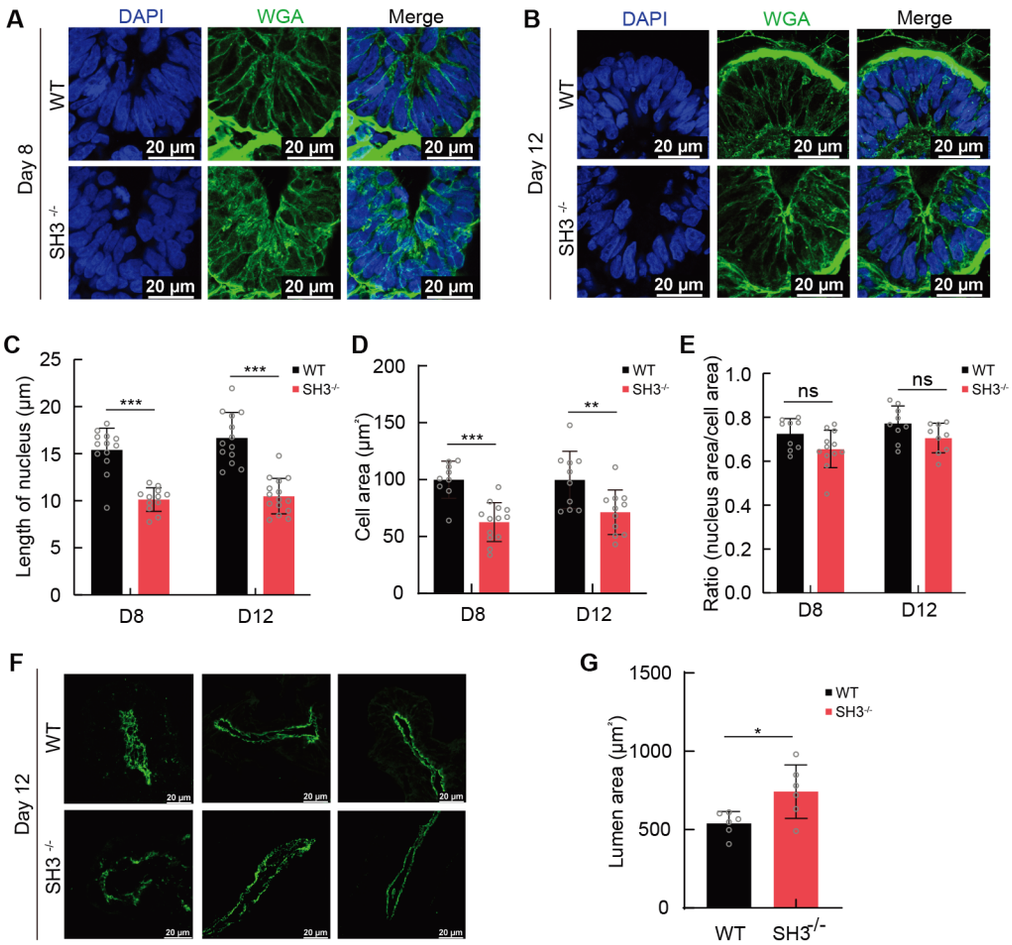

Figure 2 Effects of *SHROOM3* KO on neuroepithelial cell morphology

A, B: Representative images of WGA staining on days 8 (A) and 12 (B) of differentiation. C: Quantification results showing nuclear length on days 8 and 12 of differentiation. D: Quantification results showing cell area on days 8 and 12 of differentiation. E: Quantification results showing nucleus-to-cell area ratio on days 8 and 12 of differentiation. F: ZO-1 staining showing lumen area in WT and *SHROOM3* KO brain organoids on day 12. G: Quantification of lumen area. Data are mean±*SD*, *: P<0.05; **: P<0.01; ***: P<0.001; ns: not significant.

We further investigated the impact of inhibiting ROCK1 and F-actin on the localization of F-actin, myosin II, and PMLC. Results showed that ROCK1 inhibition reduced the apical localization of F-actin, PMLC, and myosin II (Supplementary Figure S3A–C). F-actin inhibition led to pronounced alterations in cell morphology (Supplementary Figure S3D) and disruption of F-actin, PMLC, and myosin II localization (Supplementary Figure S3D, E). Collectively, these results indicate that inhibiting either the Rho pathway or F-actin effectively replicates the phenotypic alterations observed in the *SHROOM3* KO models.

RNA-seq verified the role of *SHROOM3* in regulating neuroepithelial cell morphology

We performed transcriptome sequencing on WT and *SHROOM3* KO neuroepithelial organoids. Hisat2 was used to align the sequencing data to the reference genome and StringTie was used to obtain the gene expression matrix of each sample (Pertea et al., 2016). The DESeq2 package was used for DEG analysis (Love et al., 2014). Among the DEGs identified, 1 386 were significantly up-regulated ($\log_2$fold-change>1, adjusted P<0.05) and 1 598 were significantly down-regulated in the *SHROOM3* KO group ($\log_2$fold-change<−1, adjusted P<0.05) (Figure 6A). The clusterProfiler package was then used to perform gene set enrichment analysis (GSEA) for all genes and Gene Ontology (GO) enrichment analysis for the 2 984 DEGs (Wu et al., 2021). Results showed that the DEGs were enriched in cell morphogenesis, morphogenesis of animal organs, and cell morphogenesis involved in differentiation (Figure 6B). No significant differences in the expression of polarity and adhesion-related genes were observed between WT and *SHROOM3* KO groups (Figure 6C, D).

We utilized the predefined gene sets pertaining to human neuroepithelium from the MsigDB database and used the clusterProfiler package to further substantiate the impact of SHROOM3 on neuroepithelial cells. Results showed that the gene set involved in neuroepithelial morphogenesis was down-regulated in the *SHROOM3* KO group (Figure 6E). The Protein-Protein Interaction Networks in the String database showed an interaction relationship between SHROOM3 and ROCK1 (Figure 6F). Taken together, the transcriptomic data support the conclusion that *SHROOM3* KO affects neuroepithelial cell morphology.

DISCUSSION

NTDs constitute a major cause of neonatal mortality and morbidity. However, the mechanisms underlying the majority of gene mutations associated with NTDs remain elusive,

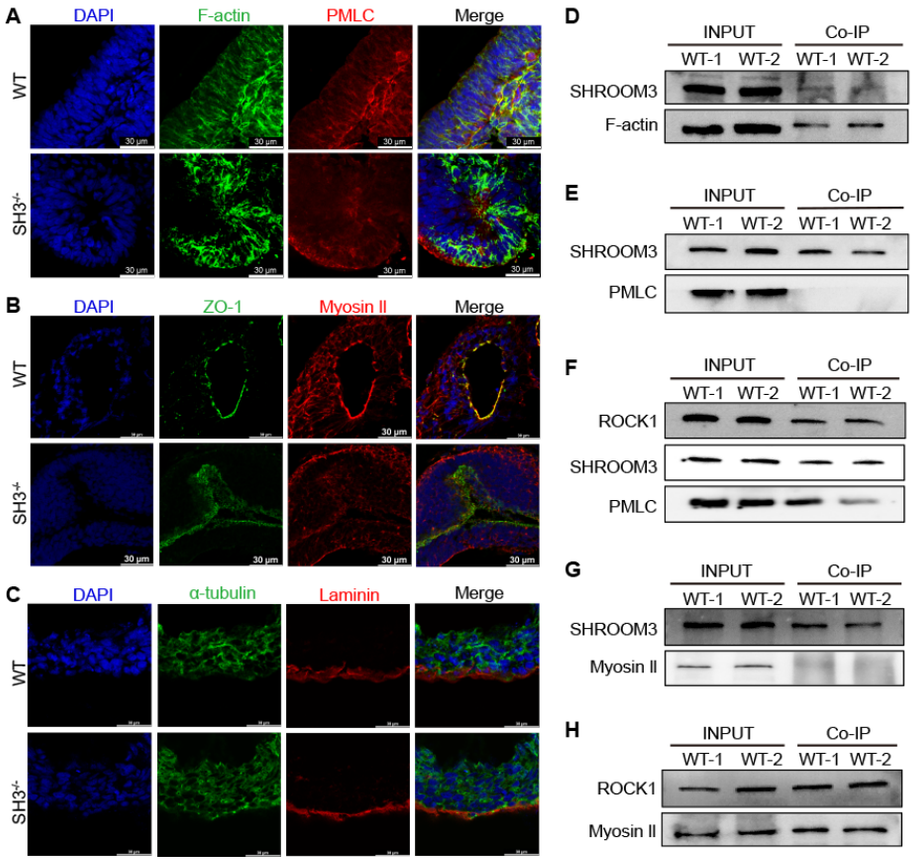

Figure 3 SHROOM3 regulates neuroepithelial cell morphology by regulating apical localization of PMLC, myosin II, and F-actin

A: Representative immunofluorescence images of F-actin and PMLC on day 12 of differentiation. B: Representative immunofluorescence images of ZO-1 and myosin II. C: Representative immunofluorescence images of α-tubulin and laminin. D: Co-IP showing interactions between SHROOM3 and F-actin. E: Co-IP showing interactions between SHROOM3 and PMLC. F: Co-IP showing interactions between ROCK1 and SHROOM3 or PMLC. G: Co-IP showing interactions between SHROOM3 and myosin II. H: Co-IP showing interactions between ROCK1 and myosin II.

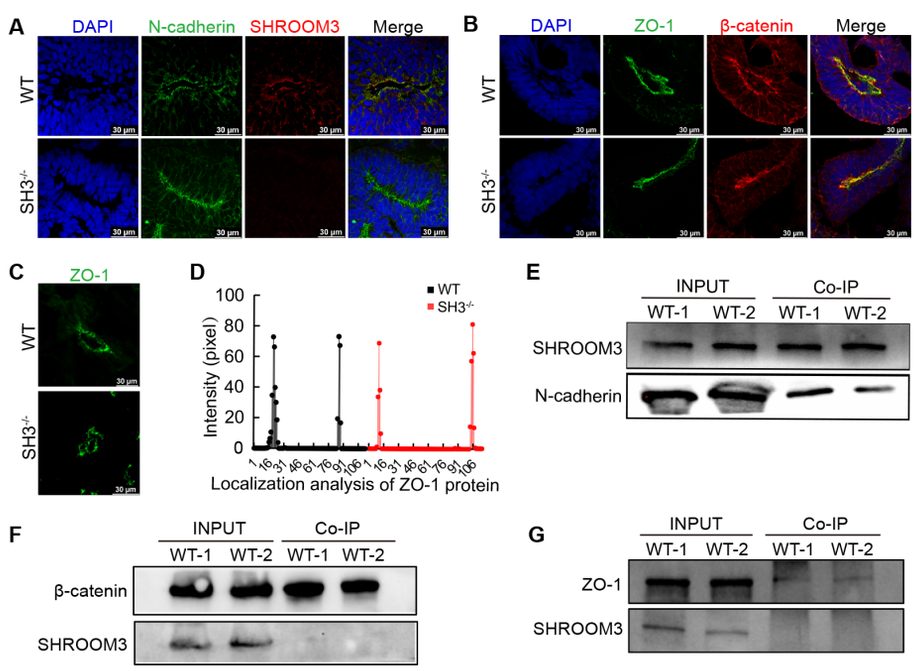

Figure 4 *SHROOM3* KO does not affect adhesion and polarity of neuroepithelial cells

A: Representative immunofluorescence images of colocalization of N-cadherin (green) and SHROOM3 (red) in apical region. B: Representative immunofluorescence images of colocalization of ZO-1 (green) and β-catenin (red). C: Representative immunofluorescence images of ZO-1. D: Fluorescence localization analysis of ZO-1 showing no difference between the two groups. E: Co-IP showing interactions between SHROOM3 and N-cadherin. F: Co-IP showing interactions between β-catenin and SHROOM3. G: Co-IP showing interactions between ZO-1 and SHROOM3.

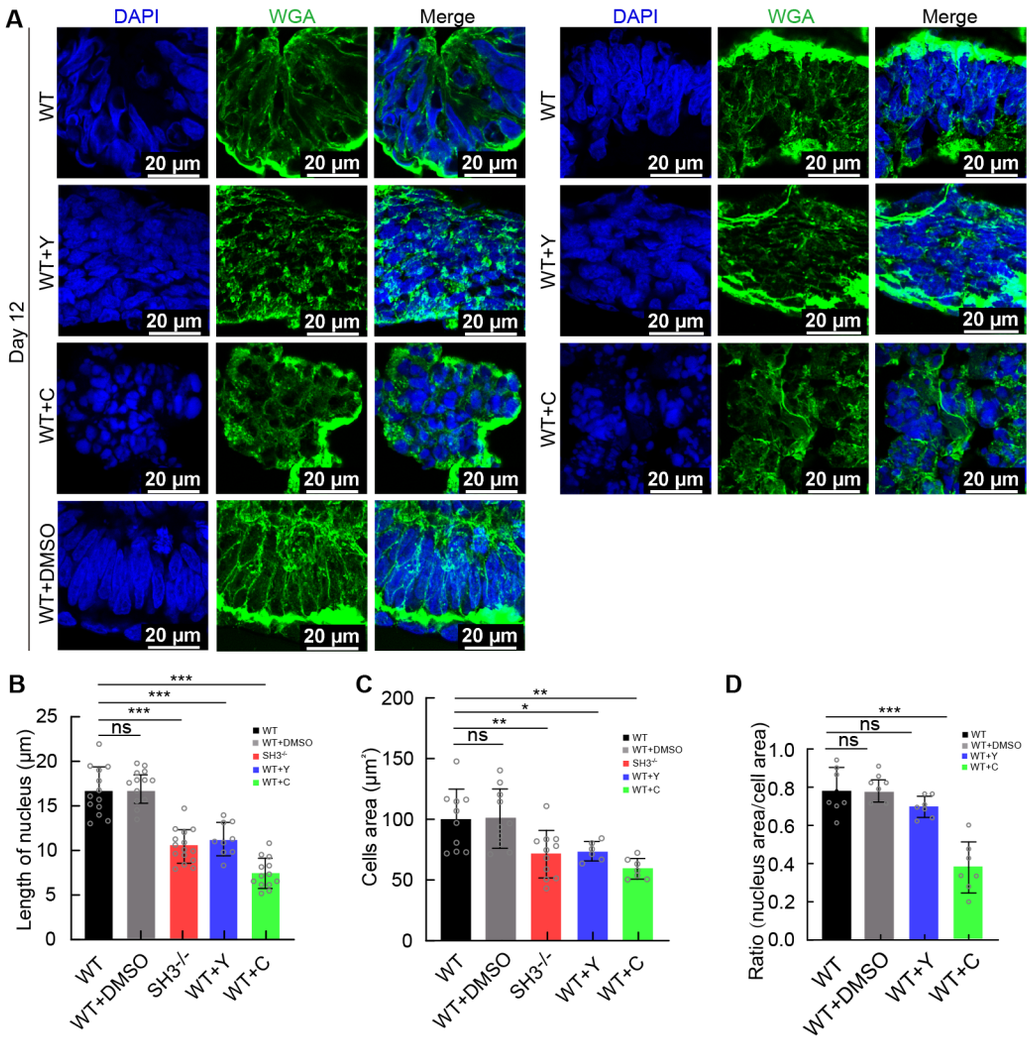

Figure 5 Inhibition of ROCK or F-actin reproduces phenotypes of *SHROOM3* KO

A: Representative WGA staining images of WT, WT+Y, WT+C, and WT+DMSO on day 12 after treatment. B: Quantification results showing length of nucleus in (A). C: Quantification results showing cell area in (A). D: Quantification results showing nucleus-to-cell area ratio in (A). Data are mean±*SD*, *: *P*<0.05; **: *P*<0.01; ***: *P*<0.001; ns: not significant. Y: Y27632 (ROCK inhibitor); C: Cytochalasin B (F-actin inhibitor).

largely due to the lack of suitable experimental models. NHPs are highly similar to humans in terms of genetic background and brain development. Here, we knocked out the *SHROOM3* gene in cynomolgus monkey embryos, generated ESCs, and constructed neuroepithelial organoids *in vitro*. We focused our analysis on brain organoids harvested on days 8 and 12, corresponding to the early stages of brain development during which SHROOM3 protein expression is prominent. Our results showed that *SHROOM3* KO induced morphological changes in neuroepithelial cells at a stage roughly equivalent to the neural plate phase *in vivo*. Compared to WT neuroepithelial cells, *SHROOM3* KO neuroepithelial cells were smaller and the nucleus was shortened. Our organoid culture system effectively recapitulated both the structural and microenvironmental features observed *in vivo*. We clearly observed the polarity at the top of the apical side and noted that the cell connections were three-dimensional (3D). Furthermore, *SHROOM3* KO led to alterations in the lumen area of the neuroepithelium, indicating a role for SHROOM3 in regulating apical contraction in these cells. The results obtained from our cynomolgus monkey organoids align closely with previous research conducted on human organoids (Takla et al., 2023), suggesting a conserved function of SHROOM3 across species. Our findings indicate that abnormalities associated with NTDs may manifest during the early neuroepithelial stage, prior to neural tube closure.

Previous studies have reported that high-dose folate supplementation in *Shroom3* mutant mice can be beneficial in the short-term but detrimental in the long-term. In contrast, our experiments using neuroepithelial organoids revealed that folate supplementation had no significant effect on neuroepithelial cell morphology, consistent with clinical reports showing that mutations in *SHROOM3* are not ameliorated by folate administration (Deshwar et al., 2020).

Previous studies have reported that SHROOM3 plays an essential role in neural tube closure by regulating the distribution of myosin II (McGreevy et al., 2015). Although Shroom3-induced apical retraction has been identified as essential for hinge point formation during neural tube closure in *Xenopus* species (Haigo et al., 2003), the underlying mechanisms remain unknown. Our findings revealed that *SHROOM3* KO led to alterations in the apical retraction of the cytoskeletal proteins myosin II, F-actin, and PMLC, thereby influencing the spatial distribution of these proteins and

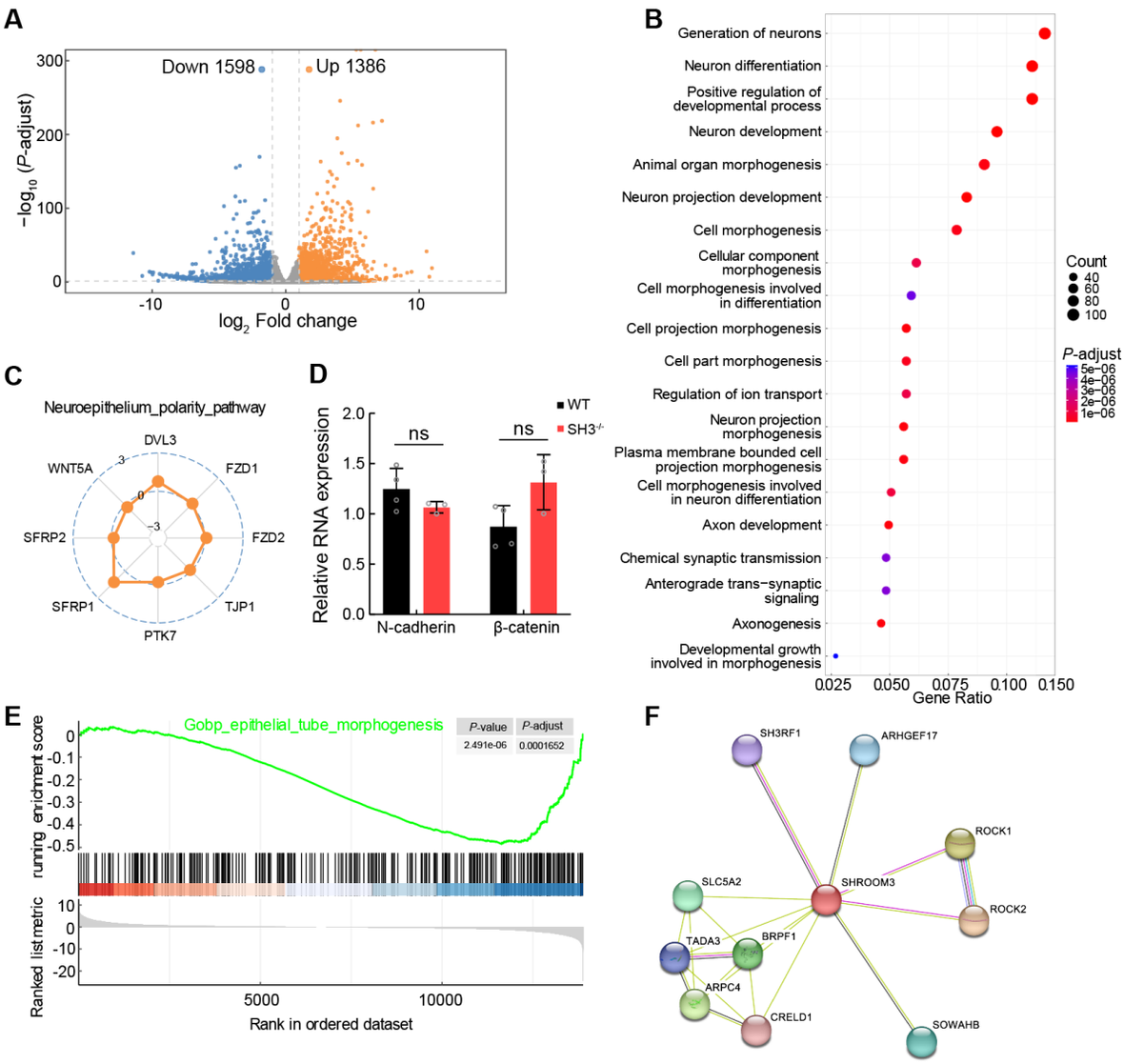

Figure 6 RNA-seq analysis reveals that *SHROOM3* gene mutations affect neuroepithelial cell shape

A: Volcano plot showing 1 386 up-regulated DEGs and 1 598 down-regulated DEGs. B: GO enrichment analysis. C: Polarity analysis of neuroepithelial cells showing no significant difference in gene expression between *SHROOM3* KO and WT groups. Orange dots indicate differences in gene expression (log_2fold-change) between *SHROOM3* KO and WT groups. D: No significant difference was found in relative RNA expression of N-cadherin and β-catenin between *SHROOM3* KO and WT groups. E: GSEA showed that the gene set involved in neuroepithelial morphogenesis was down-regulated in the SHROOM3 KO group. F: Protein-Protein Interaction Networks in the String database showed a relationship between SHROOM3 and ROCK1.

consequently affecting cell morphology. ROCK1 is a recognized downstream effector of SHROOM3. Previous studies have indicated that the interaction between SHROOM3 and ROCK1 is essential for neural tube morphogenesis in E9.5 mice embryos (Das et al., 2014). Our data confirmed the critical role of ROCK1 in mediating the function of SHROOM3 in primates and revealed that *SHROOM3* initiates the regulation of downstream F-actin and myosin II at the neuroepithelial stage, thereby exerting its regulatory effects at a very early stage of neural development.

Brain organoids have been widely used in mechanistic studies of neurological diseases. Unlike 2D cultures, 3D cultures can more accurately reflect the spatial characteristics of cells, such as the localization of skeleton proteins, cell morphology, and cell-cell interactions. Furthermore, organoids offer a viable platform for large-scale drug screening, thus accelerating the clinical translation of drugs. Despite its advantages over 2D culture systems, our 3D culture system cannot fully replicate the dynamic aspects of neural tube closure. Therefore, future work should explore the integration of organoids with biomaterials to better mimic this dynamic process. Further comparative analysis with embryonic development *in vivo* is required to determine the extent to which these *in vitro* findings accurately reflect *in vivo* conditions.

CONCLUSIONS

We established a brain organoid culture system of cynomolgus monkeys to study the effects of SHROOM3 on neural tube development. Our study revealed that, as early as the neuroepithelial stage, SHROOM3 regulates cell shape by influencing the apical localization of cytoskeletal proteins,

while not affecting polarity and adhesion proteins. This study expands our understanding of the mechanisms underlying the occurrence of NTDs that cannot be prevented by folate administration.

DATA AVAILABILITY

RNA sequencing data have been deposited in the NCBI (PRJNA1029382), China National Center for Bioinformation (PRJCA020595), and Science Data Bank databases (DOI：10.57760/sciencedb.j00139.00075).

SUPPLEMENTARY DATA

Supplementary data to this article can be found online.

COMPETING INTERESTS

The authors declare that they have no competing interests.

AUTHORS' CONTRIBUTIONS

Y.C.C., P.L., and Z.B.W. conceived the project. T.Z. and R.W. established the ES cell lines. J.Y.Z. performed the RNA-seq data analysis. P.L., R.W., and Y.Z. performed the experiments. S.G.L. and J.J.W. conceptualized the research and provided critical feedback. P.L., Y.C,C., and W.T.G. wrote the manuscript. All authors read and approved the final version of the manuscript.

ACKNOWLEDGMENTS

We thank Zhen Zhang for help in immunohistochemical staining.

REFERENCES

Benito-Kwiecinski S, Giandomenico SL, Sutcliffe M, et al. 2021. An early cell shape transition drives evolutionary expansion of the human forebrain. *Cell*, **184**(8): 2084−2102.e19.

Burckhardt CJ, Minna JD, Danuser G. 2021. Co-immunoprecipitation and semi-quantitative immunoblotting for the analysis of protein-protein interactions. *STAR Protocols*, **2**(3): 100644.

Chen XW, Sun GQ, Tian E, et al. 2021. Modeling sporadic alzheimer's disease in human brain organoids under serum exposure. *Advanced Science*, **8**(18): 2101462.

Chen YC, Wang ZB, Xie YH, et al. 2012. Folic acid deficiency inhibits neural rosette formation and neuronal differentiation from rhesus monkey embryonic stem cells. *Journal of Neuroscience Research*, **90**(7): 1382−1391.

Copp AJ, Stanier P, Greene NDE. 2013. Neural tube defects: recent advances, unsolved questions, and controversies. *The Lancet Neurology*, **12**(8): 799−810.

Das D, Zalewski JK, Mohan S, et al. 2014. The interaction between Shroom3 and Rho-kinase is required for neural tube morphogenesis in mice. *Biology Open*, **3**(9): 850−860.

Deshwar AR, Martin N, Shannon P, et al. 2020. A homozygous pathogenic variant in *SHROOM3* associated with anencephaly and cleft lip and palate. *Clinical Genetics*, **98**(3): 299−302.

Gomes AR, Fernandes TG, Vaz SH, et al. 2020. Modeling rett syndrome with human patient-specific forebrain organoids. *Frontiers in Cell and Developmental Biology*, **8**: 610427.

Greene NDE, Copp AJ. 2014. Neural tube defects. *Annual Review of Neuroscience*, **37**: 221−242.

Haigo SL, Hildebrand JD, Harland RM, et al. 2003. Shroom induces apical constriction and is required for hingepoint formation during neural tube closure. *Current Biology*, **13**(24): 2125−2137.

Huang M, Yang J, Li P, et al. 2021. Embryo-engineered nonhuman primate models: progress and gap to translational medicine. *Research*, **2021**: 9898769.

Kang Y, Zhou Y, Li YJ, et al. 2021. A human forebrain organoid model of fragile X syndrome exhibits altered neurogenesis and highlights new treatment strategies. *Nature Neuroscience*, **24**(10): 1377−1391.

Lancaster MA, Renner M, Martin CA, et al. 2013. Cerebral organoids model human brain development and microcephaly. *Nature*, **501**(7467): 373−379.

Love MI, Huber W, Anders S. 2014. Moderated estimation of fold change and dispersion for RNA-seq data with DESeq2. *Genome Biology*, **15**(12): 550.

Marean A, Graf A, Zhang Y, et al. 2011. Folic acid supplementation can adversely affect murine neural tube closure and embryonic survival. *Human Molecular Genetics*, **20**(18): 3678−3683.

McGreevy EM, Vijayraghavan D, Davidson LA, et al. 2015. Shroom3 functions downstream of planar cell polarity to regulate myosin II distribution and cellular organization during neural tube closure. *Biology Open*, **4**(2): 186−196.

Nikolopoulou E, Galea GL, Rolo A, et al. 2017. Neural tube closure: cellular, molecular and biomechanical mechanisms. *Development*, **144**(4): 552−566.

Pertea M, Kim D, Pertea GM, et al. 2016. Transcript-level expression analysis of RNA-seq experiments with HISAT, StringTie and Ballgown. *Nature Protocols*, **11**(9): 1650−1667.

Smith HM, Khairallah SM, Nguyen AH, et al. 2021. Misregulation of cell adhesion molecules in the *Ciona* neural tube closure mutant *bugeye*. *Developmental Biology*, **480**: 14–24.

Takla TN, Luo JH, Sudyk R, et al. 2023. A shared pathogenic mechanism for valproic acid and *SHROOM3* knockout in a brain organoid model of neural tube defects. *Cells*, **12**(13): 1697.

Tan T, Wu J, Si CY, et al. 2021. Chimeric contribution of human extended pluripotent stem cells to monkey embryos *ex vivo*. *Cell*, **184**(8): 2020–2032.e14.

Tang XY, Xu L, Wang JS, et al. 2021. DSCAM/PAK1 pathway suppression reverses neurogenesis deficits in iPSC-derived cerebral organoids from patients with Down syndrome. *Journal of Clinical Investigation*, **131**(12): e135763.

Velasco S, Kedaigle AJ, Simmons SK, et al. 2019. Individual brain organoids reproducibly form cell diversity of the human cerebral cortex. *Nature*, **570**(7762): 523−527.

Wu TZ, Hu EQ, Xu SB, et al. 2021. clusterProfiler 4.0: a universal enrichment tool for interpreting omics data. *The Innovation*, **2**(3): 100141.

Zalewski JK, Mo JH, Heber S, et al. 2016. Structure of the shroom-rho kinase complex reveals a binding interface with monomeric shroom that regulates cell morphology and stimulates kinase activity. *Journal of Biological Chemistry*, **291**(49): 25364−25374.

Zhu XQ, Li B, Ai ZY, et al. 2016. A robust single primate neuroepithelial cell clonal expansion system for neural tube development and disease studies. *Stem Cell Reports*, **6**(2): 228−242.